

# Non-close-packed Breath Figures via Ion Partitioning Mediated Self-Assembly

Jia En Aw,<sup>†</sup> Glen Tai Wei Goh,<sup>†</sup> Shengnan Huang,<sup>†</sup> Michael R. Reithofer,<sup>#</sup> Aaron Zhenghui Thong,<sup>‡</sup> Jia Min Chin<sup>†##\*</sup>

J. E. Aw, G. T. W. Goh, S. Huang, J. M. Chin

<sup>†</sup> Institute of Materials Research and Engineering (IMRE), 3 Research Link, 117602, Singapore.

M. R. Reithofer, J. M. Chin

<sup>#</sup> Department of Chemistry, University of Hull, HU6 7RX, Hull, United Kingdom.

E-mail: [j.chin@hull.ac.uk](mailto:j.chin@hull.ac.uk)

A. Z. Thong

<sup>‡</sup> Department of Materials, Imperial College London, SW7 2AZ, London, United Kingdom.

Keywords: non-close packed, breath figures, ion partitioning, self-assembly, pore arrays

## Abstract

We report a one-step method of forming non-close-packed (NCP) pore arrays of micron- and submicron-pores using chloroform-based solutions of polystyrene acidified with hydrogen bromide for breath figure (BF) patterning. As breath figure patterning takes place, water vapor condenses onto the polystyrene solution, forming water droplets on the solution surface. Concurrently, preferential ion partitioning of hydrogen bromide leads to positively charged water droplets which experience inter-droplet electrostatic repulsion. Self-organization of charged water droplets under surface flow, and subsequent evaporation of the droplet templates result in ordered BF arrays with pore separation-to-diameter ( $L/D$ ) ratios of up to 16.5. Evidence from surface potential scans show proof for preferential ion partitioning of

HBr. Radial distribution functions and Voronoi polygon analysis of pore arrays show that they possess a high degree of conformational order. Past fabrication methods of NCP structures typically require multi-step processes. In contrast, we have established a new route for facile self-assembly of previously inaccessible patterns, which comprises of only a single operational step.

## 1 Introduction

Breath figure (BF) patterning is a self-assembly technique to fabricate macro-porous polymer films. Aitken<sup>1</sup> and Rayleigh<sup>2</sup> first studied this phenomenon as investigations of water condensate patterns. Ensuing investigations by other groups focused on the growth of breath figures on solid substrates,<sup>3-9</sup> and subsequently, on liquid substrates such as oils.<sup>10,11</sup> Nevertheless, interest in BF patterning only expanded after François *et al.* discovered that casting carbon disulphide solutions of star-polystyrene produced highly ordered hexagonal pore arrays.<sup>12</sup>

BF patterning appeals as a straightforward route to porous polymer films,<sup>13-17</sup> whereby polymer solutions are dried in humid air. Upon drying, films with ordered hexagonal arrays of pores are formed. BF patterning is useful for fabricating separation membranes,<sup>18</sup> catalysis,<sup>19</sup> microarrays,<sup>20</sup> and even anti-reflective coatings.<sup>21</sup> Microstructures across the film can also be manipulated, or used as a template in soft lithography to form a wide range of products such as microdots and OLED patterns.<sup>22,23,24</sup> Despite the apparent simplicity of BF patterning, the actual processes underpinning this method are complex, involving solvent evaporation and water condensation, which induce and are affected by convective currents arising from concentration, temperature and surface tension gradients. In addition, the patterns formed are sensitive to casting conditions such as relative humidity,<sup>25</sup> polymer architecture,<sup>26</sup> solvent and substrate<sup>27</sup> etc., leading to disparate observations by different research groups. As such, there has been much debate regarding the exact mechanisms and

factors involved in achieving ordered BF patterns.<sup>28-33</sup> Nonetheless, the general mechanism is understood as follows: upon casting a polymer solution prepared with a volatile solvent, solvent evaporation cools the solution surface. When the solution surface temperature falls below dew point, water vapour from ambient air condenses onto the solution surface and the resulting water droplets grow in size through condensation and coalescence.<sup>10</sup> Subsequently, fluid transport mechanisms such as the Marangoni currents and thermocapillary effects then help to pack the water droplets into close-packed (CP) arrays.<sup>28-30,34,35</sup> Each droplet acts as a structural template while the polymer solution solidifies around it. No additional step is required to remove these structural templates, as they conveniently evaporate away, leaving behind imprints of CP pore arrays with pore diameters in the range of 0.2 to 20  $\mu\text{m}$ .<sup>36</sup>

One limiting aspect of BF patterning is that the arrays tend to be close-packed, with whereas non-close-packed (NCP) configurations being difficult to access. It would be desirable to controllably obtain NCP BF arrays, since NCP configurations could be useful for preventing cross-contamination in microwell assays,<sup>37</sup> or for 2D pore arrays to serve as moulds for imprinting NCP nanodot arrays via soft lithography.<sup>38</sup> NCP configurations may also improve the optical properties of 3D inverse opal photonic crystals.<sup>39</sup> Studies of NCP structure fabrication have been largely outside the field of BF templating. Current routes typically require multiple fabrication steps,<sup>40-44</sup> which can be costly and time-consuming. As such, we propose the use of BF patterning, an economical one-step technique to produce NCP porous microstructures via self-assembly.

Previously, our group reported the fabrication of NCP pore arrays via *in situ* thermal reversal of BFs, whereby the shrinkage of pores along with the water droplet templates led to NCP pore arrays (Figure S1).<sup>45</sup> However, the conformational order of NCP domains was limited by asymmetric pore shrinkage and non-uniform lateral movement of the water droplets across the solution surface.

Herein, we report a one-step method to fabricate NCP BF patterns with high conformational order and domain sizes up to several hundred microns wide. This is achieved by introducing electrostatic repulsion between templating water droplets. The drive to minimize overall electric potential energy arranges the droplets into NCP patterns with long-range order on the polymer solution surface.<sup>46-49</sup> After drying, these water droplet arrays afford NCP pore arrays in the resulting polymer film.

In order to induce inter-droplet electrostatic repulsion, we utilized preferential ion partitioning to afford electrostatic charges in water droplets during BF patterning. Hydration energy variations across different ionic species can result in preferential partitioning of one ionic species over another from the organic phase into the water phase. For example, when  $H^+$  and  $Br^-$  ions are present in an oil/water two-phase system, it is more energetically favourable for  $H^+$  ions (hydration free energy of  $-1099 \text{ kJ mol}^{-1}$ ) to migrate into the water phase over  $Br^-$  ions (hydration free energy of  $-326.6 \text{ kJ mol}^{-1}$ ).<sup>46-48</sup> We theorized that BF patterning of polymer solutions containing ions with different hydration energies (e.g.  $H^+$  and  $Br^-$ ) would result in the water droplets gaining a net positive charge, as illustrated in Figure 1a and 1b. This therefore incurs electrostatic repulsion between neighbouring water droplets and provides a means of fabricating NCP BF arrays.

## 2 Experimental

In this study, polystyrene (PS) dissolved in chloroform/toluene was acidified by adding glacial acetic acid (AcOH) containing 33 wt% hydrogen bromide (HBr) to obtain solution  $Y_{HBr/AcOH}$ . Polymer films with BF patterns were cast from  $Y_{HBr/AcOH}$ . Films were also cast from a similar solution acidified with glacial AcOH ( $Y_{AcOH}$ ) and a non-acidified PS solution ( $Y$ ). 30.0  $\mu\text{l}$  of each polymer solution was drop cast on a glass coverslip floating on a water bath and left to dry. The scheme of the procedure is shown in Figure 1c. Solution

compositions can be found in Table S1. Detailed experimental procedures can be found in the supporting information.

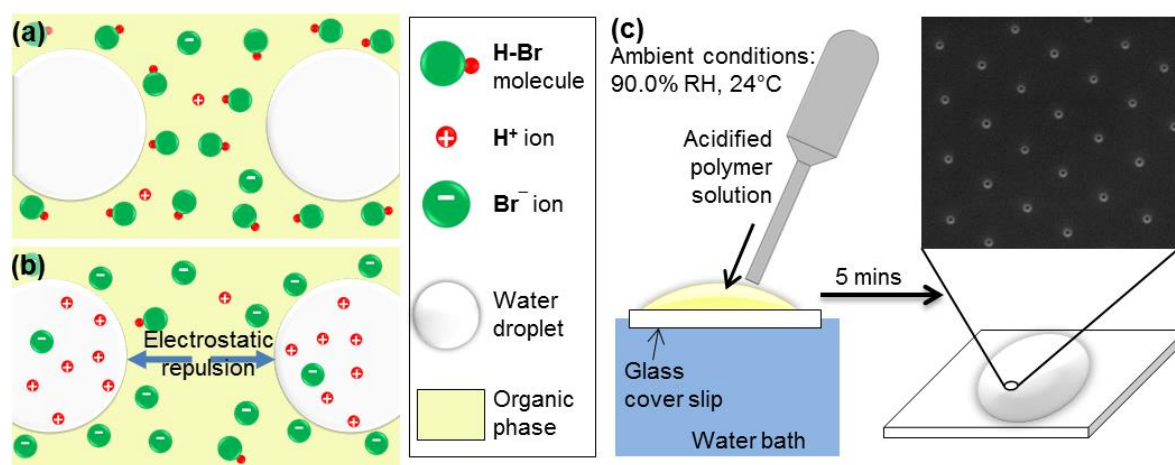


**Figure 1.** Schematics of preferential ion partitioning due to HBr present in polymer solution. (a) Before ion partitioning, HBr is dispersed in polymer solution. (b) After ion partitioning, nucleated water droplets preferentially receive H<sup>+</sup> ions, hence each gaining a net positive charge. Electrostatic repulsive forces act between neighbouring water droplets. (c) Scheme of drop-casting procedure.

### 3 Results and Discussion

To verify that preferential ion partitioning had occurred during BF patterning, surface potential (SP) imaging was performed in LiftMode on the BF patterns to map the electrostatic charge distribution. Prior to imaging, the samples were peeled off their supporting glass cover slips and placed on conductive copper adhesive tape, which served as the bottom electrode during the SP imaging. A potential difference between the tip (maintained at 10.0 nm height above the surface during the scanning) and the surface would result in an electric force on the cantilever. The tip potential is automatically adjusted to nullify the electric force. At each point, the identified tip potential is equal to the electrostatic potential at the specimen surface.

Drop-casting of  $\mathbf{Y}_{\text{HBr/AcOH}}$  led to polymer films with highly ordered, 2-dimensional NCP pore arrays as shown in Figure 2a. SP imaging of these patterns (Figure 3a) showed positive potentials at the pores, indicating the presence of positively charged residue there. When compared on a 100  $\mu\text{m}$  scale, BF patterns formed from  $\mathbf{Y}_{\text{AcOH}}$  were consistently less ordered

than those cast with  $Y_{\text{HBr/AcOH}}$  despite varying the amount of AcOH added. The BF patterns formed consisted of small domains of locally ordered NCP pores within a matrix of disordered pores, as seen by optical microscopy (Figure 2b and 2c). SP scanning on these BFs showed positive potential at the pores (Figure 3bi and 3bii), however the absence of a strong acid like HBr may decrease the extent of electrostatic repulsion, lowering the degree of order obtained in the BF patterns. On the other hand, polymer films cast from non-acidified solution  $Y$  bore only CP pore arrays and SP imaging on these arrays did not reflect an electrostatic potential signal (Figure 3c). Remaining regions of the polymer film reflect zero tip potential, pointing towards a neutral background. Overall, SP imaging of the BF patterns supports our hypothesis of preferential ion partitioning and net accumulation of  $\text{H}^+$  ions in the water phase during BF patterning with acidified PS solutions.

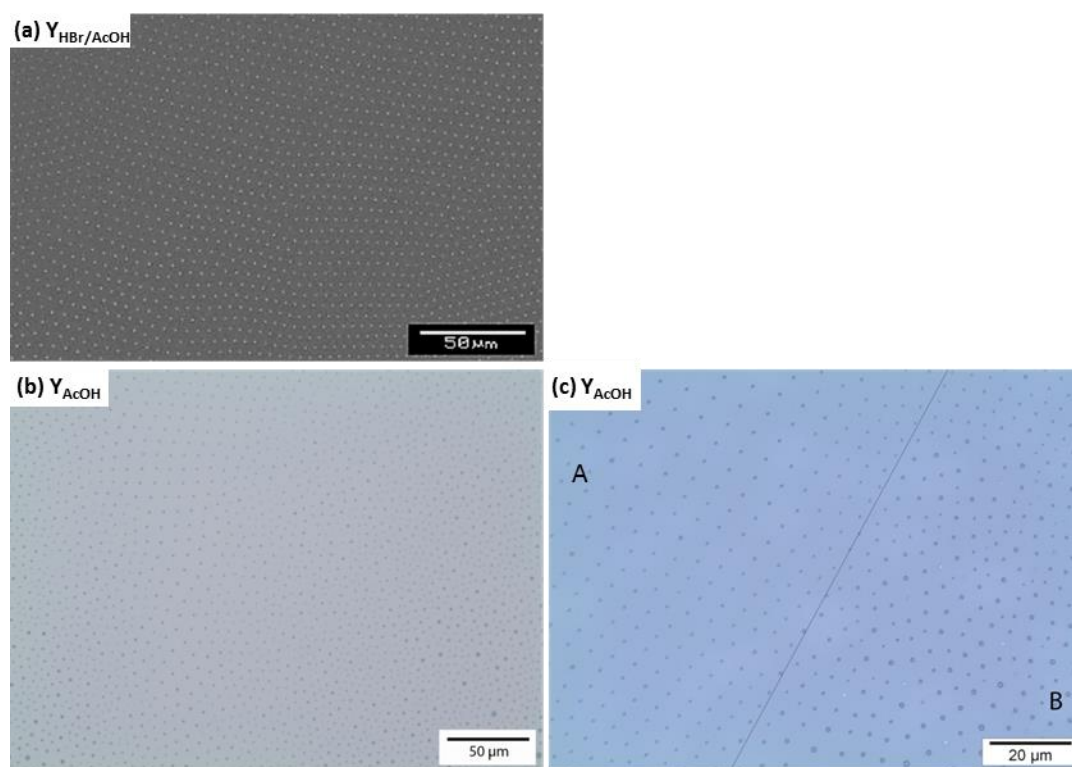


**Figure 2.** (a) SEM image of NCP pore arrays obtained from casting  $Y_{\text{HBr/AcOH}}$ . (b) Micrographs showing pores cast from  $Y_{\text{AcOH}}$ . Locally ordered NCP pore arrays were found in disordered NCP matrixes. (c) A boundary (indicated by a black line) between ordered and disordered pore regions. Region A (left side) has pores with geometric mean of 0.4826 and

geometric standard deviation of 1.1354. Region B (right side) has geometric mean of 0.5261 and geometric standard deviation of 1.3360.

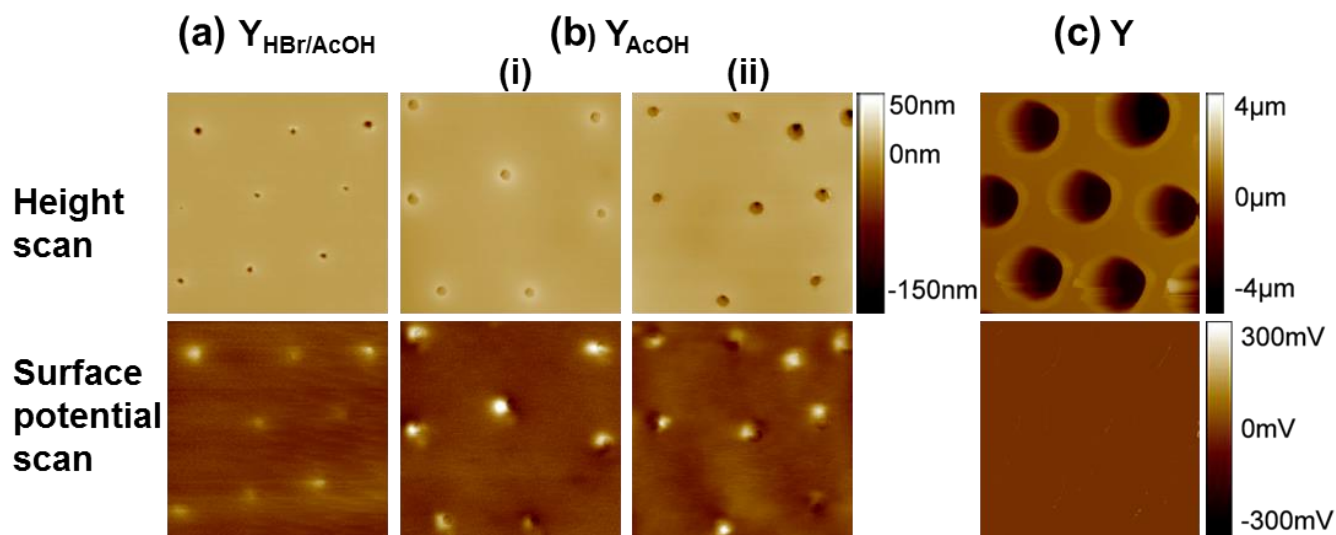


**Figure 3.** Pores were scanned using an atomic force microscope to obtain the topology (height scans) and corresponding SP images. Pores were formed by casting (a)  $Y_{\text{HBr/AcOH}}$  ( $8.3 \mu\text{m} \times 8.3 \mu\text{m}$ ), (bi, bii)  $Y_{\text{AcOH}}$  ( $11.1 \mu\text{m} \times 11.1 \mu\text{m}$ ,  $12.3 \mu\text{m} \times 12.3 \mu\text{m}$ ), and (c)  $Y$  ( $23.7 \mu\text{m} \times 23.7 \mu\text{m}$ ). The scales for height scans in (a), (bi) and (bii) are shared while the scales for all SP scans are shared.

We also observed that the electrostatic charges in BF patterns decay over several hours after polymer casting. This is unsurprising, as charges on insulator surfaces may dissipate through several mechanisms such as surface conductance, or the adsorption/desorption of ionic water clusters from ambient humid air.<sup>50-52</sup>

Positive electrostatic charges may also be detected outside the pores (Figure 3bii). This presumably occurs when water droplets undergo thermal reversal and shrink, leaving behind charged residue ( $\text{H}^+$  ions) in the vicinity of the final shrunken pore. The direction of healing by such pores may therefore be visualized, particularly when the charges reside predominantly towards one side of the pore.

We found that the use of a water bath was essential in reproducing NCP patterns. The water bath, with its high heat capacity relative to the glass slip, could moderate temperature fluctuations by serving as a heat source. To investigate this, Solution  $Y_{\text{HBr/AcOH}}$  was cast on

glass substrates of two different thicknesses (1 mm and 0.1 mm) as illustrated in Figure 4a. The thermal profiles of the droplets were recorded at intervals of 3 seconds and displayed in Figure 4b. IR thermographs of drop cast polymer solutions consistently showed radial temperature profiles that are cooler towards the droplet center and warmer at the droplet circumference (Figure 4b). As the temperature of surface fluid has an inverse relation with the surface tension, therefore a colder region on the solution surface will experience higher surface tension than a warmer region. This results in surface fluid moving from warmer to cooler regions, carrying condensed water droplets (if present) with it; this is widely known as the Marangoni effect.<sup>53</sup> Therefore, we expect surface fluid to flow radially inwards to the cooler solution center, in a converging manner as illustrated in Figure 4c. This is in line with our observation that BF patterns were typically concentrated at the center of the circular films. Comparing the thermal profiles of solutions cast on the glass substrates of different thickness (Figure 4d), we see that solution cast on the thicker glass substrate (glass thickness,  $t_{\text{glass}} = 1$  mm) took a significantly longer time to warm up to room temperature than that cast on a thinner glass substrate ( $t_{\text{glass}} = 0.1$  mm). Since the thicker glass thermally insulates the polymer solution from the water bath more efficiently than the thinner glass substrate, differences in the thermal profiles of the evaporating polymer solutions serve to illustrate the heat exchange effects of the water bath. Comparison between both thermal profiles at 21 seconds (Figure 4e) shows that polymer solution on the thinner glass (minimum temperature,  $T_{\text{min}} = 22.2$  °C) experienced milder temperature variations than polymer solution on the thicker glass (minimum temperature,  $T_{\text{min}} = 21.7$  °C), suggesting that the water bath moderates spatial temperature differences in the polymer solution, thereby mitigating temperature-induced Marangoni currents. Conversely, similar experiments performed in the absence of a water bath led to CP BF patterns, as strong Marangoni convection forces

overcame the electrostatic repulsive forces between water droplets, compacting the droplets into CP configurations.

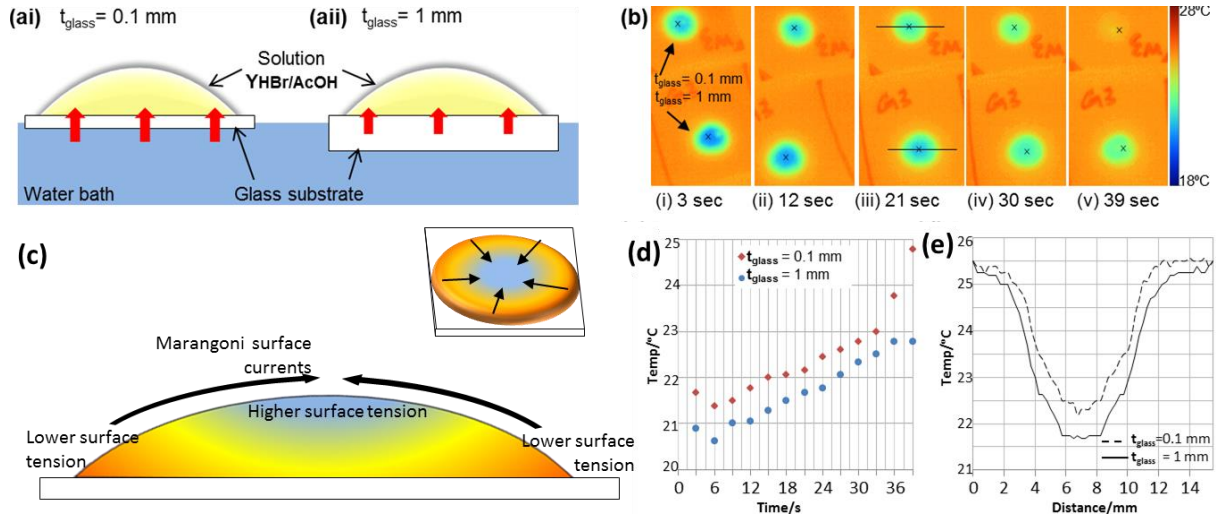


**Figure 4.** (a) Illustration depicts the heat transfer across floating glass substrates cast with polymer solution. Red arrows represent direction of heat transfer. (i) At  $t_{\text{glass}} = 0.1 \text{ mm}$ , the water bath act as heat source and thermal energy is conducted across the thin glass substrate. (ii) At  $t_{\text{glass}} = 1 \text{ mm}$ , the thick glass insulates the cool polymer solution from the water bath. (b)  $\text{YHBr/AcOH}$  was cast at the same time on two glass substrates ( $t_{\text{glass}} = 0.1 \text{ mm}$  and  $1 \text{ mm}$ ). 3D thermal profiles of both polymer solutions at (i) 3 seconds, (ii) 12 seconds, (iii) 21 seconds, (iv) 30 seconds, and (v) 39 seconds. (c) Drawing of polymer solution droplet, cross-sectional side view. The colour profile is included to illustrate the approximate temperature profile. The colder center has greater surface tension than areas around the circumference, thus leading to fluid moving (Marangoni surface currents) radially inwards. 3D view is shown on the top right. (d) Lowest temperatures on polymer solution (marked by crosses in (bi-bv)) plotted against time. (e) Cross-sectional thermal profiles of polymer solutions at 21 seconds (marked by black lines in (biii)).

To further examine the mechanism which determines whether CP or NCP pores are formed,  $\text{Y}$  and  $\text{YHBr/AcOH}$  were cast and observed under an optical microscope. Unfortunately, we could not capture a video or a series of still images of the rapid process, especially at high magnification, due to motion blur. Nevertheless, we observed in the casting of  $\text{Y}$  (Figure 5a), that water droplets randomly nucleate all over the solution surface and subsequently converge, becoming compacted wall-to-wall by Marangoni currents. This observation is in line with the

findings of others, who identified Marangoni effects as the dominant fluid mechanism in their BF experiments.<sup>28,35</sup> In the casting of  $\mathbf{Y}_{\text{HBr/AcOH}}$  (Figure 5b), NCP pores similarly begin with (I) random nucleation of water droplets. Surface currents push the water droplets together (II). However, instead of aggregating, the droplets settle at positions with some distance away from each other. Despite Marangoni currents, the droplets appear to retain their positions relative to each other until the film solidifies. These findings suggest that convergent fluid forces are counteracted by electrostatic repulsive forces between charged droplets. Interestingly, the inter-droplet distances are highly uniform across large areas, which we believe is worthy of future investigation.

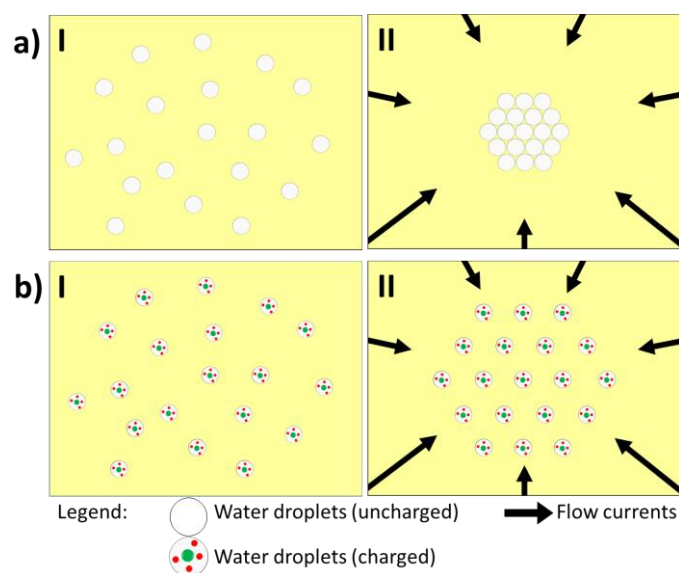


**Figure 5.** Illustrations of BF formation. (a) Upon casting  $\mathbf{Y}$ , (I) water droplets randomly nucleate on solution surface. (II) Marangoni currents converge water droplets towards the film center and pack uncharged droplets wall-to-wall. (b) Similarly, when casting  $\mathbf{Y}_{\text{HBr/AcOH}}$ , (I) water droplets randomly nucleate as well. However, (II) fluid forces are counteracted by electrical repulsive forces between charged droplets. Water droplets settle in equilibrium positions with equal inter-distances.

In order to form NCP pores, high ion mobility is necessary for  $\text{H}^+$  ions to migrate into the water phase. We assisted the migration of ions by dissolving PS in a solvent mixture of chloroform and toluene, rather than only chloroform. When the acidified polystyrene solution

only contained chloroform as the solvent, relatively CP arrays with  $L/D$  ratios of less than 3 were formed (Figure S2). Addition of toluene, which is less volatile than chloroform, would slow the drying of the polymer solution and delay its concomitant increase in viscosity,<sup>35, 54</sup> therefore allowing sufficient time for ion partitioning as well as rearrangement of the water droplets.<sup>55</sup> The optimized ratio of PS to chloroform and toluene can be found in the supporting information.

To further characterize the polymer films, optical microscopy, scanning electron microscopy (SEM) and TappingMode atomic force microscopy were performed. Several parameters were defined to facilitate analysis of the obtained BF patterns: (I)  $L$  — the separation distance between pores, measured as the pore centre-to-centre distance; (II)  $D$  — the pore diameters; and (III)  $L/D$  ratio. Conventional BF patterning forms CP pore arrays with  $L/D$  ratios close to 1, as illustrated in Figure 6a. It should be noted that unlike the close-packing of spherical particles, close-packing of pores must give an  $L/D$  ratio  $> 1$ , because the pore walls constitute a finite distance between pores. In contrast, an illustration of a NCP array is given in Figure 6b.

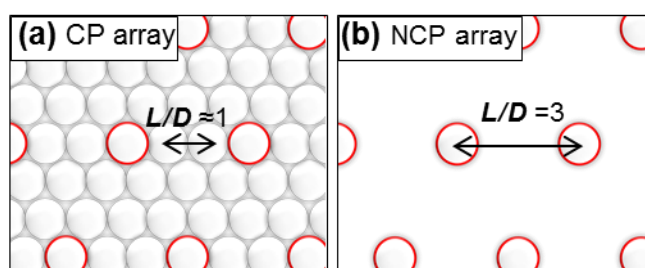


**Figure 6.** Illustration of (a) close-packed arrays ( $L/D \approx 1$ ) vs (b) non-close-packed arrays ( $L/D = 3$ ).

A measure of the orderedness of a BF array is its conformational entropy,  $S$ , which varies inversely with array orderedness.  $S$  may be obtained through Voronoi analysis of the BF arrays and calculated as  $-\sum P_n \ln P_n$ , where  $P_n$  is the probability of having a pore with  $n$

number of immediate pore neighbours.<sup>27</sup> ~~Error! Bookmark not defined.~~<sup>56-59</sup> For a completely random pattern,  $S = 1.71$ , while for perfectly ordered features,  $S = 0$ .

Solution  $Y_{HBr/AcOH}$  castings form NCP pore arrays existing in highly ordered domains spanning distances of several hundred microns (Figure 2a). Lattice orientation and separation distances of the pores maintained uniformly across each domain. Apart from the typical hexagonal pore patterns, rhombohedral patterns may also be observed (Figure 7).

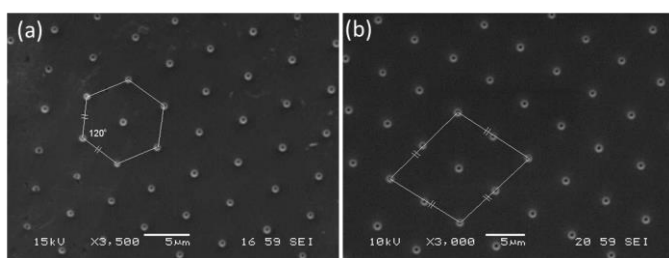


**Figure 7.** Pore arrays were observed to form two types of configurations with high order: (a) hexagonal and (b) rhombohedral patterns.

The NCP pore arrays possessed  $S$  values as low as 0.1278 (Figure 8a and 8b), indicating higher conformational order than CP BF pore arrays reported by other groups.<sup>27</sup> ~~Error! Bookmark not defined.~~<sup>57,58</sup> This result is especially remarkable since the NCP pore arrays display high  $L/D$  ratios of up to 16.5 — the highest  $L/D$  ratio achieved via BF patterning to date. Furthermore, distribution of neighbouring pores is preserved to at least second order for the array, as seen from the periodic peaks in the radial distribution function (RDF) plot in Figure 8c.

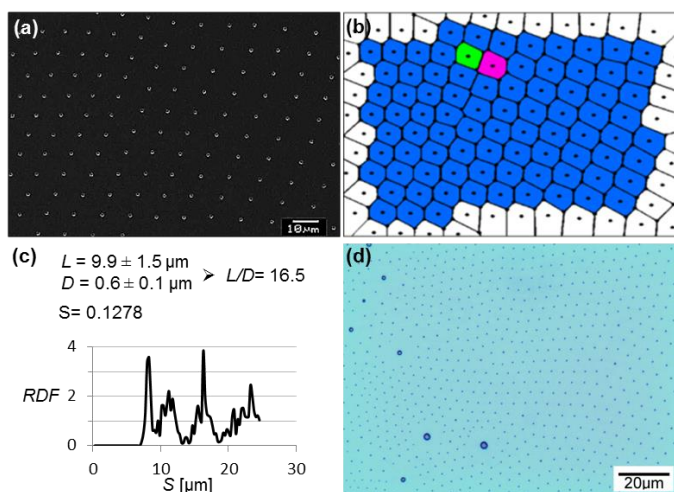


**Figure 8.** (a) SEM micrograph of a NCP pore array. (b) Voronoi diagram of pores in (a). Polygons labeled in colors green, blue, and pink represent 5, 6, and 7-sided polygons respectively. Polygons along the edge of the micrograph are excluded from the calculation of conformational entropy. (c) Measured feature sizes and RDF plot from (a). (d) Micrograph of ordered pore arrays cast from  $Y_{\text{HBr/AcOH}}$ . Point defects with larger pore sizes exhibit larger separation distances to their neighboring pores.

We found that when casting non-acidified solution  $Y$ , ordered CP domains obtained typically extend less than 100  $\mu\text{m}$ . The orderly CP packing is disrupted by boundary defects arising from the collision and imperfect alignment of droplet aggregates.<sup>36</sup> In contrast, films cast from  $Y_{\text{HBr/AcOH}}$  displayed NCP pore domains that extended up to several hundred microns. Charged water droplets tend to minimize electrical potential energy by arranging themselves into ordered arrays,<sup>47,48</sup> which provides an impetus for misalignment correction during droplet packing, thus enlarging the domain sizes of ordered arrays.

The NCP pores are much smaller than CP pores as seen from Figure 8a and 9. ( $D = 0.6 \mu\text{m}$  and  $3.1 \mu\text{m}$ ). Electrical repulsion prevents charged droplets from coming into contact and coalesce. Thus, growth of NCP water droplets is largely due to condensation and not coalescence, which serves to decrease the overall sizes of the water droplets and therefore the resulting pore sizes in the BF patterns. By limiting coalescence, we observed that across entire films, pore sizes in the NCP arrays were more uniform compared to the CP arrays. This

is in agreement with the findings of several groups that coalescence decreases pore size uniformity.<sup>30,34,35</sup>**Error! Bookmark not defined.**

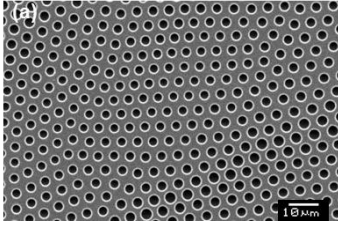


**Figure 9.** SEM micrograph of a CP pore array. Feature sizes measured from the micrograph afford the following values:  $L = 6.2 \pm 0.5 \mu\text{m}$ ;  $D = 3.1 \pm 0.2 \mu\text{m}$ ;  $L/D = 2.0$

Furthermore, it was observed that water droplet polydispersity disrupts the ordered packing of pore arrays. This holds true not just for CP arrays (whereby the order-disrupting effects of polydispersity are self-evident),<sup>35</sup> but also for our NCP patterns. For example, Figure 3b shows that the pores were more monodisperse in the ordered regions (geometric standard deviation,  $\sigma_g$ , of pore sizes = 1.1354) compared to pores in the disordered regions ( $\sigma_g$  of pore sizes = 1.3360). (See Figure 10 for pore size distribution curves) In addition, defective pores – pores with larger diameters than general pores – appear to have larger separation distances from its neighbouring pores (Figure 8d). The observation suggests that larger water droplets accumulate greater charges, resulting in greater inter-droplet electrostatic repulsion and larger separation distances.

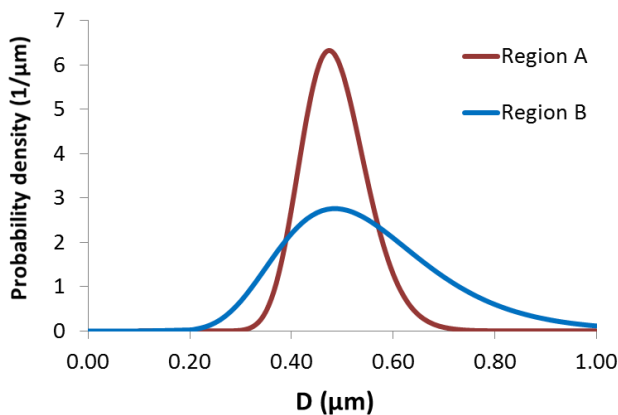


**Figure 10.** Probability distribution curves describing the pore size distributions of Region A and Region B from Figure 3b. A log normal distribution was used. Region A evidently shows higher uniformity in pore sizes as compared to Region B.

#### 4 Conclusions

In summary, we demonstrated a one-step bottom-up approach of breath figure patterning whereby preferential ion partitioning mediates the one-step self-assembly of NCP pore arrays with high **L/D** ratios of up to 16.5. Besides achieving high **L/D** ratios, the BF arrays possess high conformational order with **S** (conformational entropy) values as low as 0.1278. SP results qualitatively show that these NCP pore arrays possess positively charged residue, indicating the preferential migration of  $H^+$  ions into the water phase. The consequent electrostatic repulsive forces between water droplets cause them to align into 2D NCP ordered arrays, and to template the resulting BF patterns possessing long range order.

We have formed 2D arrays of acid-laced pores which may be exploited as economical wet etching masks for NCP patterns. In addition, for pore arrays used as microwells, aside from minimizing cross-contamination during bioassays,  $H^+$  remnants can provide an acidic environment for specific processes, or actively hold oppositely charged particles or molecules deposited in each pore. Furthermore, this method may be further explored and extended for the fabrication of 3D NCP inverse opals, and is of general interest as a direct way of forming non-close-packed structures.

#### ASSOCIATED CONTENT

##### Supporting Information

Supporting Information Available: Experimental details and supplementary figures. This material is available free of charge via the Internet at <http://pubs.acs.org>.

## AUTHOR INFORMATION

### Corresponding Author

\*Jia Min Chin, University of Hull. Cottingham Rd, Hull, Yorkshire HU6 7RX, United Kingdom. Email: [J.Chin@hull.ac.uk](mailto:J.Chin@hull.ac.uk).

### Author Contributions

The manuscript was written through contributions of all authors. All authors have given approval to the final version of the manuscript.

## ACKNOWLEDGEMENTS

This work has been supported by the Agency for Science, Technology, and Research (A\*STAR) and the Porous Materials Laboratory, Institute of Materials Research and Engineering. We thank Mr. Tristan Tan for helpful discussions. We also thank Dr. Sivashankar Krishnamoorthy for his loan of the humidity chamber, Mr. Cham Thow Min Jerald and Dr. S. Safari for reading the manuscript.

## REFERENCES

- 
- (1) Aitken, J. Breath Figures. *Proc. R. Soc. Edinburgh* **1893**, *20*, 294-296.
  - (2) Rayleigh, L. Breath Figures. *Nature*, **1911**, *86*, 416-417.
  - (3) Beysens, D.; Knobler, C. M. Growth of Breath Figures. *Phys. Rev. Lett.* **1986**, *57*, 1433-1436.
  - (4) Briscoe, B. J.; Galvin, K. P. The evolution of a 2D constrained growth system of droplets-breath figures. *J. Phys. D: Appl. Phys.* **1990**, *23*, 422- 428.
  - (5) Derrida, B.; Godrèche, C.; Yekutieli, I. Stable distributions of growing and coalescing droplets. *Europhys. Lett.* **1990**, *12*, 385-390.

- 
- (6) Steyer, A.; Guenoun, P.; Beysens, D.; Fritter, D.; Knobler C. M. Growth of Droplets on a One-Dimensional Surface: Experiments and Simulation. *Europhys. Lett.* **1990**, *12*, 211-215.
  - (7) Steyer, A.; Guenoun, P.; Beysens, D.; Knobler C. M. Growth of droplets on a substrate by diffusion and coalescence. *Phys. Rev. A* **1991**, *44*, 8271-8277.
  - (8) Briscoe, B. J.; Galvin, K. P. An experimental study of the growth of breath figures. *Colloids Surf.* **1991**, *56*, 263-278.
  - (9) Fritter, D.; Knobler, C. M.; Beysens, D. Experiments and simulation of the growth of droplets on a surface (breath figures). *Phys. Rev. A* **1991**, *43*, 2858-2869.
  - (10) Knobler, C. M.; Beysens, D. Growth of Breath Figures on Fluid Surfaces. *Europhys. Lett.* **1988**, *6*, 707-712.
  - (11) Steyer, A.; Guenoun, P.; Beysens, D. Hexatic and fat-fractal structures for water droplets condensing on oil. *Phys. Rev. E: Stat. Phys., Plasmas, Fluids, Relat. Interdiscip. Top.* **1993**, *48*, 428-431
  - (12) Widawski, G.; Rawiso, M.; François, B. Self-organized honeycomb morphology of star-polymer polystyrene films. *Nature* **1994**, *369*, 387 – 389.
  - (13) François, B.; Pitois, O.; François, J. Polymer films with a self-organized honeycomb morphology. *Adv. Mater.* **1995**, *7*, 1041–1045.
  - (14) Maruyama, N.; Koito, T.; Nishida, J.; Sawadaishi, T.; Cieren, X.; Ijro, K.; Karthaus, O.; Shimomura, M. Mesoscopic patterns of molecular aggregates on solid substrates. *Thin Solid Films* **1998**, *327*, 854-856.
  - (15) Nishikawa, T.; Ookura, R.; Nishida, J.; Arai, K.; Hayashi, J.; Kurono, N.; Sawadaishi, T.; Hara, M.; Shimomura, M. Fabrication of Honeycomb Film of an Amphiphilic Copolymer at the Air –Water Interface. *Langmuir* **2002**, *18*, 5734 -5740.
  - (16) Karthaus, O.; Maruyama, N.; Cieren, X.; Shimomura, M.; Hasegawa, H.; Hashimoto, T. Water-Assisted Formation of Micrometer-Size Honeycomb Patterns of Polymers. *Langmuir* **2000**, *16*, 6071-6076.
  - (17) Böker, A.; Lin, A.; Chiapperini, K.; Horowitz, R.; Thompson, M.; Carreon, V.; Xu, T.; Abetz, C.; Skaff, H.; Dinsmore, A. D.; Emrick, T.; Russell T. P. Hierarchical nanoparticle assemblies formed by decorating breath figures. *Nat. Mater.* **2004**, *3*, 302-306.
  - (18) Wan, L. S.; Li, J. W.; Ke, B. B.; Xu Z. K. Ordered Microporous Membranes Templated by Breath Figures for Size-Selective Separation. *J. Am. Chem. Soc.* **2012**, *134*, 95- 98.

- 
- (19) Pessoni, L.; Lacombe, S.; Billon, L.; Brown, R.; Save, M. Photoactive, Porous Honeycomb Films Prepared from Rose Bengal-Grafted Polystyrene. *Langmuir* **2013**, *29*, 10264-10271.
- (20) Ke, B. B.; Wan, L. S.; Xu, Z. K. Controllable Construction of Carbohydrate Microarrays by Site-Directed Grafting on Self-Organized Porous Films. *Langmuir* **2010**, *26*, 8946-8952.
- (21) Park, M. S.; Kim, J. K. Broad-band Antireflection Coating at Near-Infrared Wavelengths by a Breath Figure. *Langmuir* **2005**, *21*, 11404 -11408.
- (22) Boer, B. D.; Stalmach, U.; Nijland, H.; Hadziioannou, G. Microporous Honeycomb-Structured Films of Semiconducting Block Copolymers and Their Use as Patterned Templates. *Adv. Mater.* **2000**, *12*, 1581-1583.
- (23) Bolognesi, A.; Mercogliano, C.; Yunus, S.; Civardi, M.; Comoretto, D.; Turturro, A. Self-Organization of Polystyrenes into Ordered Microstructured Films and Their Replication by Soft Lithography. *Langmuir* **2005**, *21*, 3480-3485.
- (24) Bolognesi, A.; Botta, C.; Yunus, S. Micro-patterning of organic light emitting diodes using self-organised honeycomb ordered polymer films. *Thin Solid Films* **2005**, *492*, 307-312.
- (25) Madej, W.; Budkowski, A.; Raczkowska, J.; Rysz, J. Breath Figures in Polymer and Polymer Blend Films Spin-Coated in Dry and Humid Ambience. *Langmuir*, 2008, *24*, 3517-3524.
- (26) Stenzel-Rosenbaum, M. H.; Davis, T. P.; Fane, A. G.; Chen, V. Porous Polymer Films and Honeycomb Structures Made by the Self-Organization of Well-Defined Macromolecular Structures Created by Living Radical Polymerization Techniques. *Angew. Chem., Int. Ed.*, 2001, *40*, 3428–3432.
- (27) Ferrari, E.; Fabbri, P.; Pilati, F. Solvent and Substrate Contributions to the Formation of Breath Figure Patterns in Polystyrene Films. *Langmuir* **2011**, *27*, 1874-1881.
- (28) Peng, J.; Han, Y.; Fu, Y.; Yang, Y.; Li, B. Formation of Regular Hole Pattern in Polymer Films. *Macromol. Chem. Phys.* **2003**, *204*, 125-130.
- (29) Pitois, O. François, B. Crystallization of condensation droplets on a liquid surface *Colloid Polym. Sci.* **1999**, *277*, 574-578.
- (30) Srinivasarao, M.; Collings, D.; Philips, A.; Patel, S. Three-Dimensionally Ordered Array of Air Bubbles in a Polymer Film. *Science* **2001**, *292*, 79-83.

- 
- (31) Yunus, S.; Delcorte, A.; Poleunis, C. Bertrand, P. Bolognesi, A.; Botta, C. A Route to Self-Organized Honeycomb Microstructured Polystyrene Films and Their Chemical Characterization by ToF-SIMS Imaging. *Adv. Funct. Mater.* **2007**, *17*, 1079-1084.
- (32) Barrow, M. S.; Jones, R. L.; Park, J. O.; Wright, C. J.; Williams, P. R.; Srinivasarao, M. Studies of the formation of microporous polymer films in "breath figure" condensation processes. *Mod. Phys. Lett. B*, **2008**, *22*, 1989-1996.
- (33) M. F. Schatz, G. P. Neitzel. Experiments on Thermocapillary Instabilities. *Annu. Rev. Fluid Mech.* **2001**, *33*, 93-127.
- (34) Pitois, O.; François, B. Formation of ordered micro-porous membranes. *Eur. Phys. J. B* **1999**, *8*, 225-231.
- (35) Peng, J.; Han, Y.; Yang, Y.; Li, B. The influencing factors on the macroporous formation in polymer films by water droplet templating. *Polymer* **2004**, *45*, 447-452.
- (36) Bunz, U. H. F. Breath Figures as a Dynamic Templating Method for Polymers and Nanomaterials. *Adv. Mater.* **2006**, *18*, 973-989.
- (37) Xia, Y.; Gates, B.; Yin, Y.; Lu, Y. Monodispersed Colloidal Spheres: Old Materials with New Applications. *Adv. Mater.* **2000**, *12*, 693-713.
- (38) Jiang, P. Large-Scale Fabrication of Periodic Nanostructured Materials by Using Hexagonal Non-Close-Packed Colloidal Crystals as Templates. *Langmuir* **2006**, *22*, 3955-3958.
- (39) Gaillot, D. P.; Summers, C. J. Photonic band gaps in non-close-packed inverse opals. *J. Appl. Phys.* **2006**, *100*, 113118.
- (40) Ren, Z.; Li, X.; Zhang, J.; Li, W.; Zhang X.; Yang, B. Tunable Two-Dimensional Non-Close-Packed Microwell Arrays Using Colloidal Crystals as Templates. *Langmuir* **2007**, *23*, 8272-8276.
- (41) Yan, X.; Yao, J.; Lu, G.; Li, X.; Zhang, J.; Han K.; Yang. B. J. Fabrication of Non-Close-Packed Arrays of Colloidal Spheres by Soft Lithography. *J. Am. Chem. Soc.* **2005**, *127*, 7688-7689.
- (42) Plettl, A.; Enderle, F.; Saitner, M.; Manzke, A.; Pfahler, C.; Wiedemann S.; Ziemann, P. Non-Close-Packed Crystals from Self-Assembled Polystyrene Spheres by Isotropic Plasma Etching: Adding Flexibility to Colloid Lithography. *Adv. Funct. Mater.* **2009**, *19*, 3279-3284.
- (43) Aizenberg, J.; Braun, P. V.; Wiltzius, P. Patterned Colloidal Deposition Controlled by Electrostatic and Capillary Forces. *Phys. Rev. Lett.* **2000**, *84*, 2997-3000.

- 
- (44) Zhang, J.; Yang, B. Patterning Colloidal Crystals and Nanostructure Arrays by Soft Lithography. *Adv. Funct. Mater.* **2010**, *20*, 3411-3424.
- (45) Thong, A. Z.; Lim, D. S. W.; Ahsan, A.; Goh, G. T. W.; Xu, J.; Chin, J. M. Non-close-packed pore arrays through one-step breath figure self-assembly and reversal. *Chem. Sci.* **2014**, *5*, 1375-1382.
- (46) Royall, C. P.; Leunissen, M. E.; Van Blaaderen, A. A new colloidal model system to study long-range interactions quantitatively in real space. *J. Phys.: Condens. Matter* **2003**, *15*, S3581.
- (47) Leunissen, M. E.; Zwanikken, J.; Van Roij, R.; Chaikin, P. M.; Van Blaaderen, A. Ion partitioning at the oil–water interface as a source of tunable electrostatic effects in emulsions with colloids. *Phys. Chem. Chem. Phys.* **2007**, *9*, 6405-6414.
- (48) Leunissen, M. E.; Van Blaaderen, A.; Hollingsworth, A. D.; Sullivan, M. T.; Chaikin, P. M. Electrostatics at the oil-water interface, stability, and order in emulsions and colloids. *Proc. Natl. Acad. Sci. U. S. A.* **2007**, *104*, 2585-2590.
- (49) Isa, L.; Kumar, K.; Muller, M.; Grolig, J.; Textor, M.; Reimhult, E. Particle Lithography from Colloidal Self-Assembly at Liquid-Liquid Interfaces. *ACS Nano* **2010**, *4*, 5665-5670.
- (50) Rezende, C. A.; Gouveia, R. F.; Da Silva, M. A.; Galembeck, F. Detection of charge distributions in insulator surfaces. *J. Phys.: Condens. Matter* **2009**, *21*, 263002.
- (51) Gouveia, R. F.; Bernardes, J. S.; Ducati, T. R.; Galembeck, F. Acid–Base Site Detection and Mapping on Solid Surfaces by Kelvin Force Microscopy (KFM). *Anal. Chem.* **2012**, *84*, 10191-10198.
- (52) Burgo, T. A. D. L.; Rezende, C. A.; Bertazzo, S.; Galembeck, A.; Galembeck, F. Electric potential decay on polyethylene: Role of atmospheric water on electric charge build-up and dissipation. *J. Electrostat.* **2011**, *69*, 401-409.
- (53) Scriven, L. E.; Sternling, C. V. The Marangoni Effects. *Nature* **1960**, *187*, 186-188.
- (54) Li, Z.; Ma, X.; Zang, D.; Shang, B.; Qiang, X.; Hong, Q.; Guan, X. Morphology and wettability control of honeycomb porous films of amphiphilic fluorinated pentablock copolymers via breath figure method. *RSC Adv.* **2014**, *4*, 49655- 49662.
- (55) Sharma, V.; Song, L.; Jones, R. L.; Barrow, M. S.; Williams, P.R.; Srinivasarao, M. Effect of solvent choice on breath-figure-templated assembly of “holey” polymer films. *EPL* **2010**, *91*, 38001.

- 
- (56) Steyer, A.; Guenoun, P.; Beysens, D.; Knobler, C. M. Two-dimensional ordering during droplet growth on a liquid surface. *Phys. Rev. B* **1990**, *42*, 1086-1089.
- (57) Park, M. S.; Kim, J. K. Breath Figure Patterns Prepared by Spin Coating in a Dry Environment. *Langmuir* **2004**, *20*, 5347-5352.
- (58) Limaye, A. V.; Narhe, R. D.; Dhote, A. M.; Ogale, S. B. Evidence for Convective Effects in Breath Figure Formation on Volatile Fluid Surfaces. *Phys. Rev. Lett.* **1996**, *76*, 3762-3765.
- (59) Song, L.; Sharma, V.; Park, J. O.; Srinivasarao, M. Characterization of ordered array of micropores in a polymer film. *Soft Matter* **2011**, *7*, 1890-1896.